Scattering and Diffusion of Mononucleosomal DNA: Effects of Counterion Valence and Salt and DNA Concentration

Marilyn E. Ferrari† and Victor A. Bloomfield*

Department of Biochemistry, University of Minnesota, St. Paul, Minnesota 55108

Received March 20, 1992; Revised Manuscript Received May 29, 1992

ABSTRACT: We have studied the counterion valence and salt and polyion concentration effects on the static and dynamic light scattering behavior of NaDNA and CaDNA in both the moderate salt, semidilute and the low salt ("extraordinary") regimes. We have compared our results with theoretical predictions for the effects of counterion valence and concentration on the second virial coefficient and diffusion properties of DNA and with predictions for the onset of the ordinary–extraordinary transition in flexible polyelectrolytes. Ours is the first study of the counterion valence dependence of the transition for a rodlike polyion, making this comparison possible. A higher counterion valence should screen polyion charges more effectively, decreasing electrostatic interactions between polyions. The "ordinary" diffusion coefficients are lower for CaDNA than for NaDNA and reflect the ratio of counterion valences, but the apparent linear charge densities are much lower than predicted by standard polyelectrolyte theories. The second virial coefficient, B_2, obtained from static light scattering at higher salt concentrations is also lower for CaDNA than NaDNA, consistent with more effective screening by Ca^{2+}. For both NaDNA and CaDNA, the effective polyion charge needed to explain the magnitude of B_2 is greater than predicted by polyelectrolyte theory (the opposite direction from the diffusion results). We observe a slow diffusion mode for CaDNA as well as for NaDNA, with an equal diffusion coefficient but smaller amplitude. The onset of the transition is not consistent with rules developed for flexible polyelectrolytes. We show that the slow mode could arise from small degrees of inherent polydispersity if the effective volume fraction is near unity due to an expanded DNA rod diameter at low ionic strength. We also estimate the size of a putative cluster from our diffusion results and show that the existence of a very small fraction of clustered (or aggregated) material is consistent with observations, though it is unclear how such clusters might be stabilized.

Introduction

Understanding the equilibrium and dynamic behavior of polyelectrolytes is one of the major problems in modern polymer physical chemistry. The structural aspects common to all polymers—large size and asymmetric and/or flexible conformation—are combined with long-range electrostatic interactions to pose a formidable challenge to theoretical analysis. Since most biopolymers are highly charged under physiological conditions, their polyelectrolyte properties are likely to have direct relevance to their biological functions as well as to their physical behavior in solution. Of all biological polyelectrolytes, DNA is perhaps the most studied. This is not just because it is of biological importance but also because its high charge density and relatively rigid local structure make it an excellent model system. Recent advances in preparing large quantities of relatively homogeneous, monodisperse DNA have also aided physical studies.

In this paper, we report static and dynamic light scattering studies on mononucleosomal DNA in both NaCl and $CaCl_2$ solutions over a wide range of salt and polyion concentrations. Our aim is to obtain experimental data which will enable testing of theories that deal with two regimes of solution behavior. The first is the regime of moderate or semidilute polymer concentration, in which polymer–polymer excluded-volume interactions become important and, for polyelectrolytes, are augmented by electrostatic effects. As the salt concentration decreases, the polyion diffusion coefficient increases (the fast diffusion mode). The second is the regime of very low ionic strength, in which electrostatic effects become very long-ranged and in which a very slow diffusional mode appears. This regime has been termed the extraordinary phase, and the transition leading to it is called the ordinary–extraordinary transition.[1,2] Understanding the physical mechanisms underlying the extraordinary phase has been an elusive problem.

DNA in the size range of mononucleosomal fragments, around 150–160 base pairs (bp), has been a popular molecule for such studies, since it is has a contour length near 500 Å, or one persistence length, and can therefore be modeled with some plausibility as a rigid rod for which well-developed theories are available. In this paper, we extend previous light scattering studies of mononucleosomal DNA.[3-8] We vary the ion concentration from 0.06 mM (no added salt) to 1.0 M NaCl and from 0.25 mM to 0.1 M $CaCl_2$ and the DNA concentration from 0.5 to 20 mg/mL. This DNA concentration range extends into the semidilute regime at low salt and represents a wider range than previously reported. The semidilute regime is defined to exist at concentrations above C^* where the domains of individual molecules begin to overlap; estimates[7] of C^* for mononucleosomal DNA range from ≈1.5 mg/mL at low salt to ≈20 mg/mL at high salt, since it depends on the effective volume and diameter of the polyion. We use Ca^{2+} to allow testing of counterion valence effects proposed or implied by various theories.

In the ordinary regime, we determine the second virial coefficient, B_2, from total scattering intensity measurements as a function of salt concentration and counterion valence and show that it depends on counterion valence, not simply on ionic strength. Our experimental results are in good agreement with those obtained by other workers for NaDNA but are in only moderate quantitative agreement with theoretical predictions of B_2 for rodlike polyelectrolytes. We also compare the observed diffusion coefficient with the coupled mode theories originally developed by Schurr and co-workers[2] and extended by Tivant et al.[9] to include the effects of higher counterion valence. The apparent diffusion coefficient, D_{app}, measured by dynamic laser light scattering increases and the

† Present address: Department of Biochemistry and Molecular Biophysics, Washington University, St. Louis, MO 63110.

0024-9297/92/2225-5266$03.00/0

total scattered intensity declines as the monovalent salt concentration is decreased from about 1 M. The resulting fast diffusion mode can be attributed to increases in the second virial coefficient caused by increased electrostatic interactions between polyions as the salt concentration is decreased or the polyion concentration is increased.[2,9-12] These effects depend on the counterion valence, since charges of higher valence will more effectively screen polyion charges.

The ordinary–extraordinary transition was first observed by Schurr and co-workers in polylysine solutions.[1,2] This transition since has been observed for many polyelectrolytes, including DNA,[3-5,7] tRNA,[13] bovine serum albumin (BSA),[14] poly(styrene sulfonate) (PSS),[15-19] poly(A),[20] poly(2-vinylpyridine),[21] and mononucleosomes.[22] The extraordinary regime is characterized by the coexistence of fast and slow diffusion modes as the salt is further decreased. The salt concentration, C_s, at which the slow mode appears is generally about 0.01 M NaCl, although it has been observed in salt concentrations as high as 1 M NaCl.[7] The ratio of the diffusion coefficients for the two modes, D_{fast}/D_{slow}, can be as large as 100. In some cases, the amplitude of the fast mode is very small and only the slow mode is observable at lower salt concentrations.[2,18,23] Slow modes have also been observed in solutions of neutral rodlike molecules, although at considerably higher concentrations than with polyelectrolytes.[24]

Although the general features of the fast mode are reasonably clear, the physical mechanism of the ordinary–extraordinary transition and the nature of the slow mode are still not understood despite years of study. Experimentally, a puzzling feature of the transition is that it is not manifested in other physical measurements. Conductivity[25] and intrinsic viscosity[26] measurements on polylysine as a function of salt concentration revealed only small, though significant, discontinuities and changes in the slope in the region of C_s. Electrophoretic mobilities and diffusion coefficients (D_{ELS}) obtained from electrophoretic light scattering (ELS) measurements on polylysine do not show the anomalous behavior observed in D_{app}. D_{ELS} values decrease at low salt concentration but are always greater than D_{slow}.[27,28] Schmitz and Ramsay[29] used QLS in the presence of a sinusoidal electric field (SEF-QLS) to study the effect of electric field strength on the diffusion behavior in the extraordinary phase. The slow diffusion mode is observed at low field strength, while the fast diffusion is observed at higher field strength. These results suggest that the species responsible for the slow mode is rather unstable and easily disrupted by the addition of salt or an applied electric field, or by filtration.[30] It is also possible that the slow mode represents a type of dynamic process not probed by these techniques.

There is good evidence that the slow mode does not represent center-of-mass diffusion of a single chain. Tracer diffusion coefficients measured by fluorescence photobleaching recovery on polylysine at low salt show a decrease of only about 50% in decreasing the salt concentration from 10 to 0 mM KCl.[29,31] Wang et al.[7] used forced Rayleigh scattering to measure self-diffusion coefficients (D_{self}) of mononucleosomal DNA. Values of D_{self} were 2–10 times greater than those observed for D_{slow} under the same experimental conditions and showed a relatively large DNA and salt concentration dependence not observed for D_{slow}. The diffusion coefficient associated with the slow mode has an unusual temperature dependence contrary to the expected behavior of a diffusion process; D_{slow} decreases with an increase in the temperature. Wang et al.[7] pointed out that this behavior was observed for the rotational correlation time of DNA.[32]

Several theoretical explanations have been proposed for the slow mode, but none has proved completely satisfactory. These explanations fall into four main groups, which are not mutually exclusive. These are electrostatic interactions, orientational or translational ordering, clustering, and polydispersity.

Electrostatic explanations are the most obvious, since the slow diffusion mode becomes more dominant as the ionic strength decreases. However, theories of electrostatic effects on diffusion of polyelectrolytes, such as the coupled ion theory discussed later in this paper, predict that the diffusion coefficient of the polyion will increase with decreasing salt. They therefore explain D_{fast} but not D_{slow}. Drifford and Dalbiez[18,19] have proposed a relationship (eq 25) that correlates the polymer and salt concentration dependence of the transition in the flexible polyelectrolytes, polylysine and PSS. This expression proposes that the transition will occur when the counterion concentration contributed by the polyion exceeds the concentration of the added salt. When this condition is met, the Debye–Hückel approximation for the polyion potential is no longer valid. However, the Drifford–Dalbiez equation does not hold for DNA, as we show below.

Stigter[33] suggested that the slow mode in polylysine might result from an isotropic–anisotropic transition in rodlike polyions due to repulsive polyion–polyion interactions. This explanation was based on an extension of Onsager's theory[34] for the isotropic–anisotropic transition to include an increased effective polyion diameter at low salt. For 1.5 mg/mL of DNA, the coexistence of two phases is predicted when [NaCl] $\leq$ 0.001 M, which is 10-fold below the NaCl concentration at which the slow mode is observed. Better agreement is obtained if uncondensed counterions from the DNA are included in the calculation of ionic strength.[35] However, there is no optical evidence of orientation, such as birefringence, in solutions undergoing the ordinary–extraordinary transition. Liquid crystalline order has been observed only in much more concentrated DNA solutions[36,37] than those considered here. Doi and co-workers[38] developed a random-phase approximation theory which predicts that a slow mode should occur in solutions of (uncharged) hard rods at concentrations well below the actual transition to a mesophase. This is due to concentration fluctuations coupled to orientational fluctuations and has been observed with PBLG in DMF.[24] However, numerical comparison of this theory with data on DNA, even using the augmented polyion diameter approach of Stigter, shows that the predicted effects are too small at the low DNA concentrations used.

There is considerable evidence of short-range translational ordering of polyelectrolytes at low salt from small-angle X-ray scattering (SAXS) and other scattering techniques. Recent SAXS studies[35] on mononucleosomal DNA show that the intermolecular spacing decreases with increased DNA concentration and decreases with decreasing salt concentration. The ordering disappears when salt is added; this is also observed for salt concentrations in the range of C_s for PSS.[17] The results on the salt concentration dependence are consistent with the formation of hexagonally closed-packed ordering of DNA. Static light scattering measurements show a maximum in the structure factor which coincides with a minimum in D_{app} in salt-free solutions of PSS[17] and low salt solutions of charged fd-virus.[39] SAXS measurements on polylysine,[40] polyacrylate,[41] and tRNA[13] in the presence of low salt or in the absence of added salt also show that the

position of the Bragg peak is affected by polymer size and concentration and salt concentration. Ordering of NaPSS is also indicated by NMR relaxation studies at salt concentrations corresponding to C_s. The results show that a significant population of Na^+ ions experience long-lived, slowly rotating field gradients, suggesting ordering of local domains of 100 Å or more.[42] However, all of these studies were carried out at a rather high polyion concentration, and there is no direct evidence that they are relevant to the ordinary–extraordinary transition observed at considerably lower concentrations.

A "temporal aggregate" model, in which polyion clusters of fairly well-defined size coexist with the free polyions, has been proposed by Schmitz and co-workers[43] to explain the slow mode behavior. The attractive force stabilizing the clusters is presumed to result from a fluctuating dipole field generated by the sharing of small ions by several polyions at low salt. The repulsive forces are unfavorable electrostatic interactions between polyions and random Brownian motion which favor disruption of the clusters. The model is an attractive one, but it has not been formulated theoretically in testable form, so it is not clear that the proposed balance of forces actually leads to stable clusters. A model in which purely repulsive electrostatic interactions lead to clustering was proposed by Ise et al.[41] to explain the small-angle X-ray results obtained for polyacrylate and other polyelectrolytes but has been shown by Overbeek[44] to be invalid.

If a clustering mechanism explains the slow mode, the scattering intensity might be expected to increase because of the large effective molecular weight of a cluster. In fact, however, the total scattering intensity decreases, while the scattering intensity from the slow mode remains roughly constant through the extraordinary regime.[3] Therefore, substantial reduction in the scattering power of the clusters, due to form factor and/or thermodynamic nonideality effects, must be invoked if a clustering mechanism is to be plausible.

Several theories which treat polydispersity as the cause of the slow mode have been proposed.[45-47] For nearly monodisperse DNA, a polydispersity explanation at first glance seems unlikely. However, the sample has a small variation around its mean size (160 ± 10 base pairs) whose effect might be amplified under suitable conditions. Also, cluster formation might be viewed as a type of polydispersity. In a quantitative treatment, the relaxation times and relative amplitudes of the slow and fast modes will depend on the relative sizes of the scattering species and the volume fractions which they occupy.

Materials and Methods

Sample Preparation. We used a previously described method[48] to obtain gram quantities of mononucleosomal (160 bp) DNA from calf thymus required to conveniently explore the range of DNA concentrations used in our studies.

All buffers used for light scattering were prepared with water treated by reverse osmosis and then by an in-lab five-bowl Millipore filtration system with a 0.22-μm final filter, leading to a final resistance of 18 MΩ. Buffers contained 1 mM Tris [tris(hydroxymethyl)aminomethane] and the appropriate salt concentration at pH 8. Analytical-grade NaCl or $CaCl_2$ was used in the preparation of these buffers.

DNA was extensively dialyzed against buffers containing NaCl (1 mM to 1 M) or $CaCl_2$ (0.25 mM to 0.1 M). Dialysis (4 × 500 mL) was performed on 1.5-mL samples at 4 °C over a period of 48 h for samples containing NaCl. An additional dialysis step for $CaCl_2$-containing solutions against 1 mM Tris, pH 8, was included to eliminate phosphate present in the DNA storage buffer. Mono- and divalent salt concentrations of the low-salt dialysates were verified using inductively coupled plasma (ICP) spectroscopy at the Analytical Services Laboratory, Department of Soil Science, University of Minnesota. Salt concentrations from ICP analysis were within 5% of the desired values. The lowest salinity buffer (0.06 mM NaCl) contains no added NaCl; the concentration of NaCl is determined from ICP analysis.

DNA samples and buffer blanks were filtered through Anopore 0.2-μm inorganic membranes directly into precleaned light scattering tubes. DNA concentrations after filtration were always determined spectrophotometrically by absorption at 260 nm (A_{260}) using an extinction coefficient of 20 mg^{-1} mL cm^{-1}. Samples were centrifuged prior to light scattering measurements as previously described[3] to eliminate scattering from dust. The scattering intensity remained constant (±5%) over the course of the measurements, and no detectable sample redistribution occurred as determined from A_{260} on diluted aliquots taken from the region of the scattering volume. Samples were periodically monitored for degradation during the course of the light scattering experiments by 6% polyacrylamide gel electrophoresis.

Light Scattering Apparatus and Measurements. Light scattering measurements were performed on a Lexel Model 95 argon ion laser operating at a single line power of ~150 mW using a wavelength of 488 nm. The apparatus used for these measurements has been previously described[49] and includes a Langley-Ford 1096 correlator with an ITT FW130 phototube. Measurements were made at scattering angles of 40–110°. The data from the correlator were transferred to a microcomputer for subsequent analysis. All measurements were made at 20 °C.

Dynamic Measurements and Data Analysis. The second-order photocurrent intensity autocorrelation function

$$C(\tau) = B[1 + \beta|g^{(1)}(\tau)|^2] \quad (1)$$

is the quantity measured in a homodyne dynamic light scattering experiment. B is the base-line intensity. β is an instrument constant which depends on the number of coherence areas sampled by the photomultiplier and reflects the signal to noise ratio. τ is the product of the channel time Δt and the correlator channel number. The general form of $|g^{(1)}(\tau)|$ can be expressed as a distribution function in decay rates Γ

$$|g^{(1)}(\tau)| = \int_0^\infty A(\Gamma) \exp(-\Gamma\tau)\, d\Gamma \quad (2)$$

where $A(\Gamma)\, d\Gamma$ is the contribution to the total scattering from the decay process with a rate constant between Γ and $\Gamma + d\Gamma$.

Values for the base line were determined from the average of the readings in the last eight channels, which were delayed by $64\Delta\tau$ from the first 64 channels. Correlation functions were collected with a one-channel predelay to eliminate shot noise. In the cases where channel times of less than 4 μs were used, the predelay was chosen to eliminate an instrumental artifact with a 3.6-μs decay time.[50]

Each experiment was first analyzed by the cumulant procedure[51] to assess whether $C(\tau)$ showed significant deviations from single-exponential decay. Since no single criterion is diagnostic for the presence of a bimodal distribution, deviations from single-exponential decay were assessed by several criteria: (1) Visual inspection of the correlation function revealed the presence of more than one decay process. (2) D_{app} calculated from cumulant analysis showed a strong dependence on the autocorrelator channel time. (3) Nonrandom residuals and increasing χ^2 values were obtained from cumulant analysis. (4) Random residuals and low χ^2 values were obtained from biexponential analysis. Judging the quality of the fit solely from χ^2 values will often be misleading since systematic deviations are not apparent; these are revealed by residual plots of the difference between the fitted and experimental values $C(\tau)$ as a function of τ. When the experimental function is well represented by the fitted function, the residuals should be low and randomly distributed around zero, reflecting the level of noise present.

To fit $C(\tau)$ to a double exponential, peeling analysis was first performed to obtain starting values for nonlinear fitting to the equation

$$C(\tau) = B(1 + \beta[A_s \exp(-\Gamma_s\tau) + A_f \exp(-\Gamma_f\tau)]^2) \quad (3)$$

using the Marquardt–Levenberg algorithm.[52] The experimental base line was used for B, and β was determined from cumulant

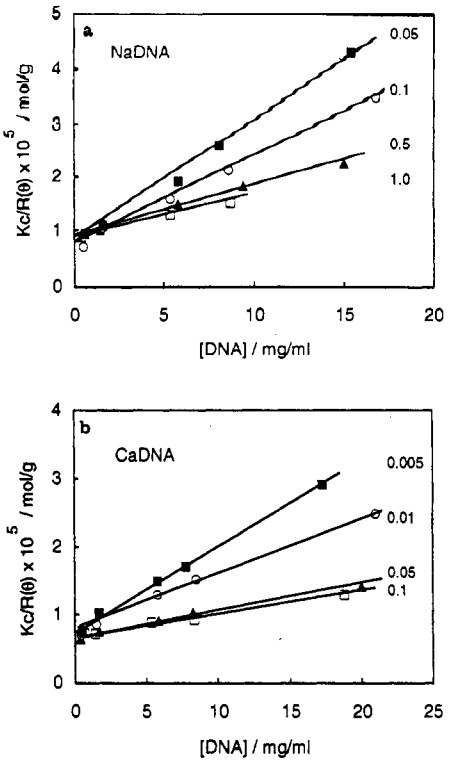

Figure 1. Dependence of $Kc/R(\theta)$ on [DNA]. (a) 0.05–1 M NaCl; (b) 5.0 mM to 0.1 M $CaCl_2$. The intercepts and slopes give apparent molecular weights M_w^{-1} and second virial coefficients B_2. As explained in the text, the M_w values were all adjusted to 105 600 and used to compute corrected B_2 values, which gave the points in Figure 2.

analysis. Testing of our data analysis routines using simulated data showed that biexponential fitting can produce reliable values for the relaxation rates and amplitudes of the decay processes expected in the ordinary–extraordinary transition if each mode can be fit with about 20 channels.

Two widely separated decays cannot be reliably fit in a single run using a 64-channel correlator. For this reason, the channel time was varied by at least a factor of 10 to better isolate the fast and slow decays. If two decay processes are present, then D_{app} will depend on the time scale (τ) chosen to measure the correlation functions. The faster and slower modes can be isolated using shorter and longer channel times, respectively. If only a single decay rate predominates, then D_{app} should not show a large channel time dependence.

The optimal range of channel time for each component was determined by collecting correlation functions at 90° using a range of channel times and then judging the quality of the fit from residual plots and χ^2 values for a double-exponential fit. The channel times for other angles were determined by keeping the product $q^2\Delta t$ constant, where q is the scattering vector, $(4\pi n_0/\lambda_0)\sin(\theta/2)$. Δt was adjusted to optimize the quality of the fit.

Total Intensity Measurements and Data Analysis. Static light scattering measurements yield the Rayleigh ratio $R_\theta = i_\theta/I_0$, the ratio of the scattered intensity per unit volume at scattering angle θ to the incident intensity.[53] For small molecules, R_θ is independent of θ. In the case of noninteracting particles in the limit of infinite dilution, the Rayleigh ratio can be written

$$R_\theta = KcM_w \tag{4}$$

where $K = \{4\pi^2 n_0^2/N_A\lambda_0^4\}(dn/dc)^2$ for vertically polarized incident light. dn/dc is the refractive index increment, M_w is the weight-average molecular weight, and c is the DNA weight concentration. At higher solute concentrations, the assumption of independent scatterers is no longer valid and inter- and intramolecular interactions affect the scattered intensity. Rearranging eq 4 and including effects of intermolecular interactions gives[6]

$$Kc/R_\theta = P(\theta)^{-1}[M_w^{-1} + 2B_2S(\theta)c + \ldots] \tag{5}$$

where B_2 is the second virial coefficient in the osmotic pressure expansion and $S(\theta)$ and $P(\theta)$ represent the inter- and intramolecular form factors, respectively.

The total intensity of scattered light was measured in 1-s increments with at least 2 sets of 10 measurements/set made for each DNA sample, buffer blank, and standard benzene solution. Deviations were typically less than 5% for each set of measurements. The excess scattered intensity of the DNA at each scattering angle for the DNA was calculated from

$$I'_{DNA}(\theta) = [I_{DNA}(\theta) - I_{buffer}(\theta)]/I_{benz}(\theta) \tag{6}$$

Values for Kc/R_θ were determined from

$$Kc/R_\theta = c(dn/dc)^2/[\alpha I'_{DNA}(\theta)] \tag{7}$$

where $dn/dc = 0.166$ cm³/mg for NaDNA.[3,5] The same dn/dc value was used for CaDNA, since corrections for CaDNA were estimated to be negligible. This assumption is reasonable, at least at high salt concentrations where the main contribution to the polarization is from the salt ions which are in excess concentration over the polyion. $\alpha = 1.847$ cm³/mol is a constant determined from the scattering geometry and the scattering properties of benzene.[54]

We used a two-variable regression analysis method to obtain values for B_2 and M_w. The relationship between these quantities is

$$Kc/R_\theta = 1/M_w + 2Bc + (1/M_w)[(16\pi R_G^2/3\lambda^2)]\sin^2(\theta/2) \tag{8}$$

where R_G is the radius of gyration. Regression analysis was performed on Kc/R_θ as a function of c and $\sin^2(\theta/2)$. This is equivalent to the standard Zimm plot analysis where two separate regression steps are performed. M_w^{-1} is obtained from the intercept, and the slope of the second regression analysis is $2B_2$.

Results and Analysis

High Salt and the Ordinary Regime. Total Light Scattering Intensity. We used light scattering to determine the second virial coefficient B_2, in order to assess the effective volume of DNA as a function of ionic strength and ion type. The angular dependence was small, since $q^2R_G^2 \approx 0.1$ for 500-Å-long DNA molecules. Experimental data are shown in Figure 1. M_w values as much as 30% higher than the 105 600 expected for a 160 bp fragment are found for CaDNA from the intercepts of these plots. We do not think that this is due to aggregation, of which the diffusion data show no evidence. We suspect that a more likely source of the discrepancy is the refractive index increment (0.166 cm³/g) assumed. Therefore, we have adjusted dn/dc to give the expected molecular weight; plausible values of dn/dc between 0.17 and 0.19 were obtained. These values were then used to compute B_2 from the slopes of the plots in Figure 1. These values are plotted as a function of ionic strength ([NaCl] or 3[$CaCl_2$]) in Figure 2. The Na values are in reasonable agreement with those obtained by Nicolai and Mandel.[6] The virial coefficients for CaDNA lie markedly below those for NaDNA at the same ionic strength, presumably because of the greater charge neutralization by Ca which reduces electrostatic repulsion.

These values of B_2 may be compared with the theoretical prediction for a rodlike polyion[6]

$$B_2 = (\pi/4)N_{av}M^{-2}d_{eff}L_{eff}^2\{1 + [(3+\pi)/2](d_{eff}/L_{eff}) + (\pi/4)(d_{eff}/L_{eff})^2\} \tag{9}$$

for which the structural diameter d and contour length L are enlarged by electrostatic effects to effective values d_{eff}

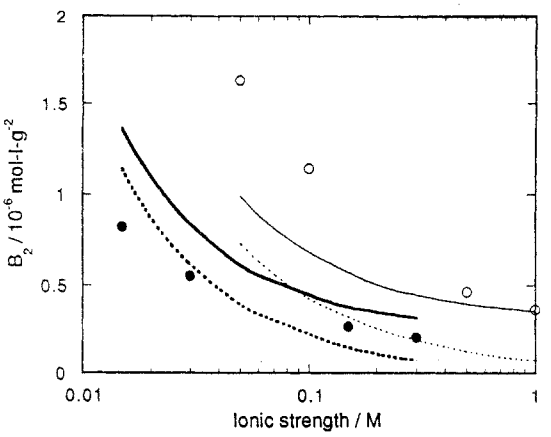

Figure 2. Second virial coefficient of 160 bp DNA as a function of ionic strength. Open circles and light lines: NaDNA. Closed circles and heavy lines: CaDNA. The circles are experimental values, corrected as described in the text. The lines are theoretical, calculated according to eqs 9–12. The dotted lines use linear charge density predicted by counterion condensation theory (eq 13). The solid lines use corrected charge density (eq 14).

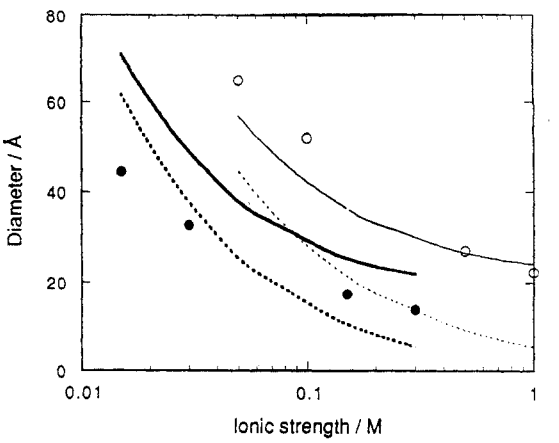

Figure 3. Effective diameter of 160 bp DNA as a function of ionic strength. Open circles and light lines: NaDNA. Closed circles and heavy lines: CaDNA. The circles indicate diameters computed from the experimental second virial coefficient. The lines are theoretical predictions from eqs 10 and 11. The dotted lines use linear charge density predicted by counterion condensation theory (eq 13). The solid lines use corrected charge density (eq 14).

and L_{eff}. The effective diameter is

$$d_{eff} = d + \kappa^{-1}(\ln Y + \gamma - {}^1/_2 + \ln 2) = d + \kappa^{-1}(\ln Y + 0.616) \quad (10)$$

where

$$Y = 2\pi\nu_{eff}{}^2 Q\kappa^{-1} \exp(-\kappa d) \quad (11)$$

Q is the Bjerrum length, $e^2/\epsilon k_B T$; κ^{-1} is the Debye length $[4\pi Q\sum_i C_i' Z_i^2]^{-1/2}$; and ν_{eff} is the effective charge density per unit length. e is the elementary charge, ϵ the solvent dielectric constant, k_B the Boltzmann constant, T the Kelvin temperature, and C_i' the concentration in ions/cm^3. When the condition $L \gg d$ is not satisfied, end effects are treated by expressing the effective length as

$$L_{eff} = L + \kappa^{-1} \quad (12)$$

According to counterion condensation theory[55]

$$\nu_{eff,cc} = (NQ)^{-1} \quad (13)$$

where N is the counterion valence. An alternative[6] uses the linearized Poisson–Boltzmann equation to obtain a correction reflecting the finite DNA radius, $a = d/2$, and influence of ionic strength

$$\nu_{eff,corr} = [NQ\kappa a K_1(\kappa a)]^{-1} \quad (14)$$

where K_1 is a modified Bessel function.

We calculated B_2 using these equations with a rise per base pair of 3.4 Å and a structural diameter d = 25 Å. The results are shown as the curves in Figure 2, with the dotted lines obtained from $\nu_{eff,cc}$ for ν_{eff} and the solid lines from $\nu_{eff,corr}$. The curves reflect the general trend of the experimental data, but the calculated values for NaDNA lie substantially below the experimental points as ionic strength decreases. Except in the limit $\kappa a \to 0$, $\nu_{eff,corr} > \nu_{eff,cc}$. Thus DNA–DNA repulsions, and B_2, are predicted to be greater for $\nu_{eff,corr}$. Agreement with experiment using $\nu_{eff,corr}$ is better for NaDNA, but $\nu_{eff,cc}$ gives better agreement for CaDNA.

The effective diameters extracted from the experimental second virial coefficients and calculated from eq 10 are shown in Figure 3. Because of lower charge neutralization, $\nu_{eff,corr}$ gives larger d_{eff}. It should be noted, however, that at high ionic strength use of $\nu_{eff,cc}$ gives $d_{eff} < d$. This unphysical result arises because Y is less than 1 at high ionic strength (large κ). In this sense, the use of simple counterion condensation theory with eq 10 is inconsistent.

Diffusion Coefficients. We measured the diffusion coefficients of NaDNA and CaDNA over a wide range of salt and DNA concentrations. In this section we report results for the ordinary diffusion coefficient, D_{ord}, obtained at high and moderate salt concentrations. We searched for evidence of a slow diffusional mode at high salt without success. Residuals from a single-exponential fit were less than 0.2% and randomly distributed around zero. Biexponential fitting did not give reproducible results, and the channel time dependence of the first cumulant was less than 10%. Deviations from expected behavior were mainly manifested in rather high values of the normalized second cumulant, $\mu_2/\langle\Gamma\rangle^2$: ca. 0.25 for NaDNA in 0.5 M NaCl and 0.1 for CaDNA in 0.1 M $CaCl_2$. These are generally taken as indicating either large polydispersity (which should not occur in these quite monodisperse preparations) or otherwise noisy signals. The source of this noise is not clear to us, since our solutions were clean and gave adequate scattering intensity. It may be due to contributions from neutral fluctuations in the NaCl concentration at high salt, though these should appear only in the first few channels under our conditions. We feel that our results are generally consistent with a single process dominating the scattering at high salt.

The diffusion coefficient of mononucleosomal DNA at high NaCl and $CaCl_2$ concentrations is plotted as a function of DNA concentration in Figure 4. The z-average diffusion coefficients measured by cumulant analysis were essentially independent of angle between 40° and 110°, so the values reported are averages over all angles. All the NaDNA points, and the CaDNA points at lower concentrations, are described fairly well by the standard linear equation

$$D_{ord} = D°(1 + k_D c) \quad (15)$$

where $D°$ is the infinite dilution diffusion coefficient and k_D is the diffusion virial coefficient. Values of $D°$ and k_D are listed in Table I. The $D°$ values are in generally good agreement with the theoretical value of 2.7×10^{-7} cm^2/s for a cylinder with 24-Å diameter and 544-Å length (160 bp × 3.4 Å/bp)[56] and the high salt $D°$ values obtained by others with similar DNA preparations.[3,5,7] The values of k_D will be discussed below.

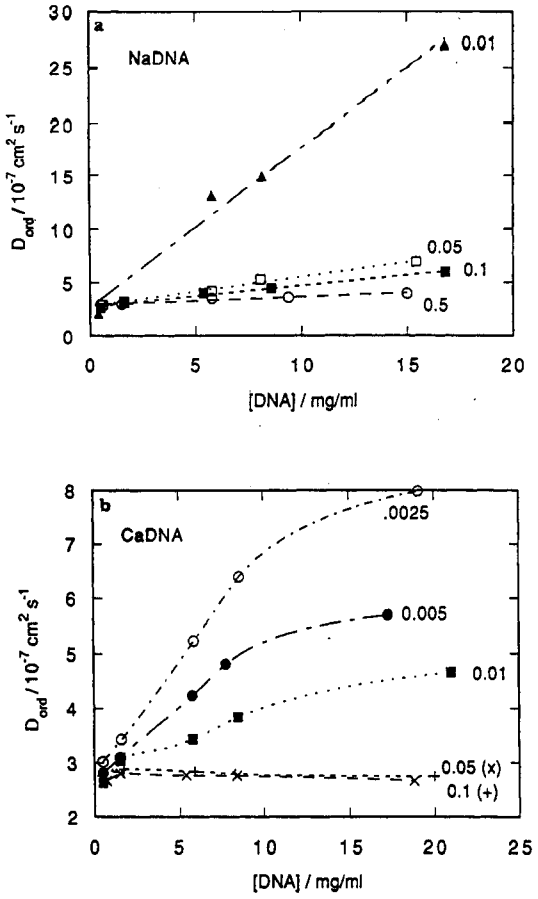

Figure 4. DNA concentration dependence of D_{ord}. (a) [NaCl] 0.01–0.5 M; (b) [$CaCl_2$] = 0.5 mM to 0.1 M.

Table I
D_0 and k_d Values Obtained from the Salt Concentration Dependence of D_{ord}

[NaCl]/ M	D_0/ (10^{-7} cm^2 s^{-1})	exptl	k_d/(L g^{-1}) for coupled ion Z_{Eff} = 32	Z_{Eff} = 26	virial
0.5	2.91 ± 0.07	0.03 ● 0.01	0.03	0.01	0.04
0.1	2.75 ± 0.12	0.07 ± 0.01	0.13	0.07	0.19
0.05	2.78 ± 0.14	0.10 ± 0.02	0.26	0.14	0.29
0.01	3.32 ± 0.99	0.43 ± 0.16	1.26	0.71	

[$CaCl_2$]/ M	$D°$/ (10^{-1} cm^2 s^{-1})	exptl	k_d/(L g^{-1}) for coupled ion Z_{Eff} = 18	Z_{Eff} = 10	virial
0.01	2.66 ± 0.11	0.06 ± 0.01	0.13	0.07	0.06
0.005	2.61 ± 0.06	0.13 ± 0.01	0.25	0.13	0.12
0.0025	2.68 ● 0.12	0.20 ± 0.02	0.49	0.26	
0.001	2.41 ± 0.10	0.43 ● 0.03	1.14	0.62	
0.0005	2.70 ± 0.10	0.41 ● 0.06	2.05	1.15	

Values of D_{app} in 0.1 M $CaCl_2$ and 1 M NaCl do not show a systematic dependence on the DNA concentration from 0.4 to 10 mg/mL. Similar results for NaDNA were obtained by Wang et al.[7] By contrast, D_{app} for NaDNA in 0.5 M NaCl increases linearly with increasing DNA concentration, in agreement with the results of Nicolai and Mandel.[5] Apparently, intermolecular interactions are manifest even at this relatively high ionic strength.

Figures 5 and 6 show the dependence of D_{ord} on NaCl and $CaCl_2$ concentrations, respectively, at [DNA] = 8.5 mg/mL. Below 0.01 M, the experimental values of D_{ord} are obtained from the D_{fast} computed from biexponential analysis on short channel data. The trend and magnitude of these values for NaDNA is consistent with results obtained by us and others.[3,5,7] These results are comprehensible in terms of standard theories of diffusion of polyelectrolytes, as discussed below.

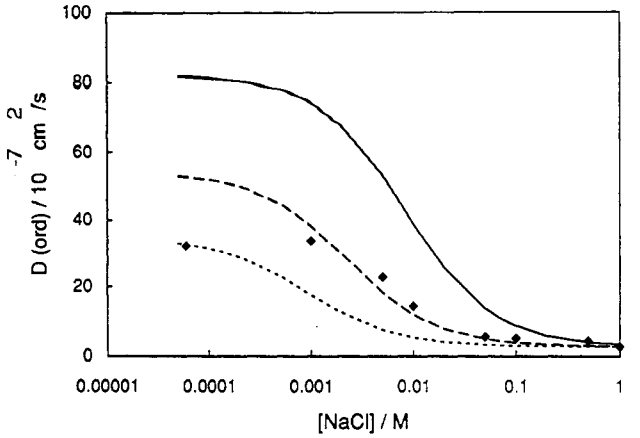

Figure 5. Comparison of the salt dependence of $D_{ord,Na}$ with theoretical predictions of coupled-ion theory at [DNA] = 8.5 mg/mL and various DNA charges Z. The points are experimental data. The lines correspond to: (—) Z = 77 (counterion condensation prediction); (- - -) Z = 32; (···) Z = 16.

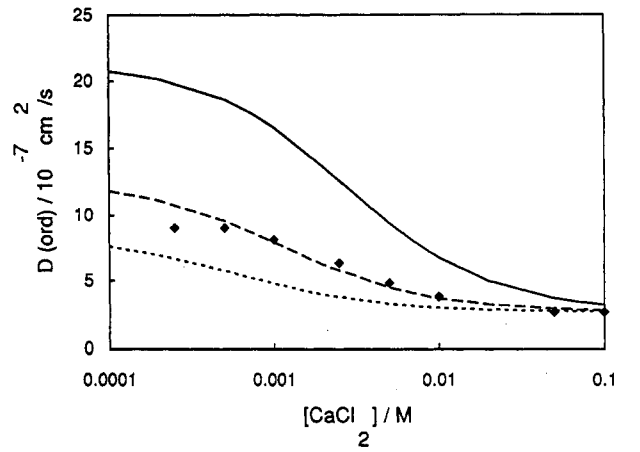

Figure 6. Comparison of the salt dependence of $D_{ord,Ca}$ with theoretical predictions of coupled-ion theory at [DNA] = 8.5 mg/mL and various DNA charges Z. The points are experimental data. The lines correspond to: (—) Z = 38 (counterion condensation prediction); (- - -) Z = 18; (···) Z = 10.

To understand these results, we consider two theories of the concentration and ionic strength dependence of D for polymers and polyelectrolytes. The first is the coupled mode theory developed by Schurr and co-workers[1,2] and a similar treatment developed by Tivant et al.[9] The latter is a generalization to include higher valence and differing mobilities of the added salt ions, enabling us to compare $D_{ord,Ca}$ and $D_{ord,Na}$. For uni-univalent salts in which the counterion and co-ion have identical diffusion coefficients D_s, these theories give identical results:

$$D_{ord} = {}^1/_2[D_p(1 - \Omega) + D_s(1 + \Omega)] \qquad (16)$$

where D_p is the high salt infinite dilution value of D_{app} for the polyion, and

$$\Omega = [D_p - X]/[D_p + X]$$

$$X = D_s[1 + (2C_s/C_p)Z_{eff}^{-1}]Z_{eff}^{-1} \qquad (17)$$

C_p and C_s are the molar concentrations of polyion and added salt, respectively, and Z_{eff} is the effective number of elementary charges on the polyion.

The generalized theory[9] which takes into account differences in ion valence and mobility gives

$$D_{app} = {}^1/_2[D_p(1-t_1) + D_2(1-t_1) + D_3(1-t_3) - \sqrt{\Delta}] \quad (18)$$

where

$$\Delta = D_p{}^2(1-t_1)^2 + D_2{}^2(1+t_2)^2 + D_3{}^2(1-t_3)^2 + 2[D_pD_2(t_1t_2-t_3) + D_2D_3(t_2t_3-t_1) + D_1D_3(t_1t_3-t_2)] \quad (19)$$

where 1–3 refer to macroion, counterion, and co-ion, respectively. The t_i are the transport coefficients of species i

$$t_i = \kappa_i{}^2D_i/\sum_i \kappa_i{}^2D_i \quad (20)$$

where the κ_i's are partial Debye–Hückel factors

$$\kappa_i{}^2 = \frac{4\pi e^2}{\epsilon k_B T} C_i' Z_i{}^2 \quad (21)$$

These expressions predict an increase in D_{ord} from its high salt value to a plateau with decreasing salt concentration, resulting from the electrostatic coupling between polyions and counterions. The low salt plateau value of D_{ord} depends on the polyion and small ion mobilities and on Z_{eff}.

The curves in Figure 5 use eqs 18–21 to calculate D_{ord} for NaDNA at 8.5 mg/mL (8.0×10^{-5} M) as a function of [NaCl] for various choices of the effective polyion charge. In all cases we used $D_p = 2.7 \times 10^{-7}$ cm^2/s, $D_2 = D_{Na^+} = 1.33 \times 10^{-5}$ cm^2/s, and $D_3 = D_{Cl^-} = 2.0 \times 10^{-5}$ cm^2/s. With 160 bp and 2 phosphate charges/bp, our DNA has a structural charge of $Z = 320$. According to counterion condensation theory (eq 13), the effective charge should be

$$Z_{eff} = Z/(NQ/b) = Z/(N\xi) \quad (22)$$

where the charge density parameter ξ is the ratio of the Bjerrum length (7.1 Å in water at 25 °C) to the charge spacing b (1.7 Å for double-stranded DNA). Thus $\xi = 4.2$, and with a counterion valence $N = Z_2$ of 1 for Na^+, $Z_{eff} = 76$. The upper, solid curve in Figure 5 is calculated with this value of Z_{eff}; it is clearly too high. The middle curve, with $Z_{eff} = 32$ (90% charge neutralization), fits the data fairly well, except at the lowest salt concentration. An even lower Z_{eff}, 16, falls significantly below the data.

Similar results are shown in Figure 6 for CaDNA, with $D_{Ca} = D_2 = 7.7 \times 10^{-6}$ cm^2/s. Here $N = Z_2 = 2$, so the counterion condensation prediction for Z_{eff} is 38. This gives calculated D_{ord}'s well above experimental results. $Z_{eff} = 18$ (94.5% charge neutralization) gives the best fit to the data, except at the lowest salt concentrations.

Thus the results for NaDNA and CaDNA are consistent, in that the effective DNA charge needed to fit the coupled-ion diffusion theory to the experimental results is more than 2-fold lower than the counterion condensation theory prediction. This lower-than-expected effective charge for NaDNA was also noted in earlier work from our group.[3] It has also been observed in electrophoretic studies of CaDNA.[57] We observe, however, that the apparent effective charge for CaDNA is about half that for NaDNA, in accord with expectations based on eq 13. The simplest reason for the deviation from coupled-ion theory is that this theory is valid only when the polyion contributes a relatively low proportion of the total mobile charge in solution. It may also be that the values of D_{ord} extracted from the experimental autocorrelation functions are somewhat less accurate than those obtained at high salt, in that they may reflect some component of slow mode behavior.

We also note that deviations between counterion condensation theory predictions of DNA charge density, and the effective charge densities needed to fit the data, are in opposite directions for the diffusion coefficients discussed in this section and the virial coefficients discussed previously. For D_{ord}, $Z_{eff} < Z_{cc}$, while for B_2, $Z_{eff} > Z_{cc}$.

We use two approaches to compare our results for the DNA concentration dependence of the ordinary diffusion behavior to theoretical predictions. The first is the coupled-ion theory discussed above. The fourth column of Table I shows k_d calculated (by varying the DNA concentration in eqs 18–21 while keeping added salt and other parameters constant) with the effective charges employed in Figures 5 and 6 that gave the best fit to the salt dependence of D_{ord}. In general, the calculated k_d's are too high and increase too rapidly with decreasing salt. The results obtained by reducing Z_{eff} (to 26 for NaDNA and 10 for CaDNA) to give a good fit at the higher NaCl and $CaCl_2$ concentrations are shown in column five of Table I. Again, the calculated k_d's seem to increase too rapidly at low ionic strength.

Our results for NaDNA may be compared with those of Wang et al.,[7] who found $Z_{eff} = 9$ for mononucleosomal DNA in the concentration range 0.1–9 mg/mL in 1 mM salt, using eqs 16 and 17. One explanation for this discrepancy is the method used to obtain D_{ord}. Wang and co-workers measured D_{ord} from the fast decay of biexponential fits to long channel data, while we obtained it from the fast relaxation of biexponential fits to short channel data. Accurate estimation of the fast decay from our long channel data was difficult because it typically decayed within the first 10 channels. Similar difficulties were reported by Nicolai and Mandel[5] at lower salt and high DNA concentrations.

The second approach to the concentration dependence of D_{ord} utilizes thermodynamic and hydrodynamic approaches directly, according to the now-standard equation (e.g., refs 5 and 8)

$$k_d = 2MB_2 - v_2 - k_f \quad (23)$$

This equation includes thermodynamics in the $2MB_2$ term (diffusion is a flow in response to a chemical potential gradient), volume conservation in the partial specific volume v_2 term (the flow of other molecules creates a back-current which retards diffusion), and hydrodynamic interaction in the k_f term. The theory of hydrodynamic interaction in solutions of rodlike molecules is not very well developed, but according to the theory of Peterson[58]

$$k_f = \frac{RTL^2}{3000\eta D^\circ M}\left(\frac{3}{8p}\right)^{2/3} \quad (24)$$

where η is the solvent viscosity and $p = L/d$ is the axial ratio of the rod. For 160 bp DNA with an assumed diameter of 26 Å, $p = 22$, $k_f = 0.056$ cm^3/g, and $v_2 = 0.556$ cm^3/g. Substitution of these values along with the experimental thermodynamic second virial coefficients (the points in Figure 2) leads to the values in the last column of Table I. Agreement with measured k_d's is fairly good in the few cases where the experimental conditions overlap.

At still lower NaCl or $CaCl_2$ concentrations, plots of D_{ord} vs [DNA] become noticeably curved, presumably indicating the increasing importance of third and higher virial coefficients as the range of effective intermolecular interaction increases.

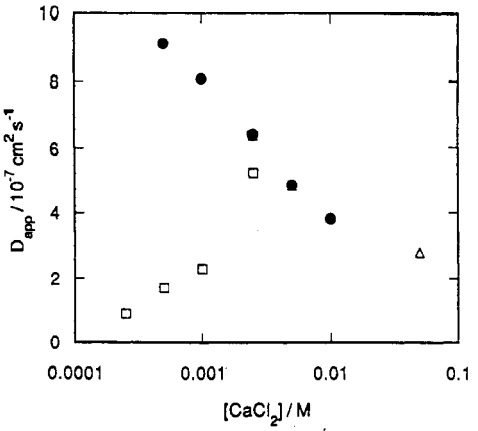

Figure 7. D_{app} calculated from cumulant analysis as a function of $CaCl_2$ concentration for data collecged at long (□), medium (△), and short (●) channel time. [DNA] = 8.5 mg/mL.

Low Salt and the Extraordinary Regime. Total Light Scattering Intensity. As the salt concentration is decreased, the scattered intensity also decreases, consistent with the general behavior observed for polyelectrolytes. Reliable estimates of M_w and B_2 were difficult in these cases due to the large deviations from linearity observed in the dependence of Kc/R_θ on $\sin^2(\theta/2)$.

Diffusion Coefficients. Since there is a large amount of evidence that two diffusion modes are present in low salt polyelectrolyte solutions, we measured D_{app} as a function of autocorrelator channel time at the lower salt concentrations. Typical channel times are Δt_{short} = 0.5–4 μs, Δt_{med} = 2–15 μs, and Δt_{long} = 6–60 μs, with $\Delta t_{long}/\Delta t_{short} \geq 10$. When a single decay rate predominates, D_{app} should not show a large channel time dependence, and correlation functions collected at long channel times should decay to the base line in a time less than $64\Delta t$. Similar channel times were used for CaDNA and NaDNA to facilitate comparison.

As the salt concentration is decreased, a marked channel time dependence of D_{app} is observed, clearly indicating the presence of more than one diffusion mode. An example is seen in Figure 7 at [$CaCl_2$] ≤ 1.0 mM with [CaDNA] ≈ 8.5 mg/mL. Data collected at long channel times show a gradual decrease in D_{app} to a value of about (1–2) × 10^{-7} cm^2/s as [$CaCl_2$] goes below 1.0 mM. For NaDNA at a comparable concentration, similar behavior is observed at [NaCl] ≤ 10 mM (data not shown) in agreement with our previously published results.[3] However, the decrease in D_{app} is more abrupt and to a smaller value of ~0.4 × 10^{-7} cm^2/s. Nicolai and Mandel[5] also noted the existence of a slow mode in autocorrelation functions obtained with [NaCl] ≤ 0.01 M.

When D_{app} shows a channel time dependence, the residuals from cumulant analysis on long channel data show large, nonrandom deviations. The autocorrelation functions are better represented as two-exponential decays, as shown in Figure 8. Biexponential fitting resulted in values for $D_{slow,Ca}$ = 0.26 (±0.02) × 10^{-7} cm^2/s and $D_{slow,Na}$ = 0.27 (±0.01) × 10^{-7} cm^2/s, independent of scattering angle and in good agreement with other measurements on mononucleosomal NaDNA.[3,7] Although slow mode diffusion coefficients are not significantly different for CaDNA and NaDNA, relative amplitudes of the slow mode contribution to the scattering, A_{slow}, differ noticeably. Figure 9 shows that $A_{slow,Ca}$ is considerably less than $A_{slow,Na}$ and that it decreases moderately but monotonically with increasing q^2, behavior consistent with scattering from a large particle or structured aggregate. This difference in the amplitudes of the slow components accounts for the

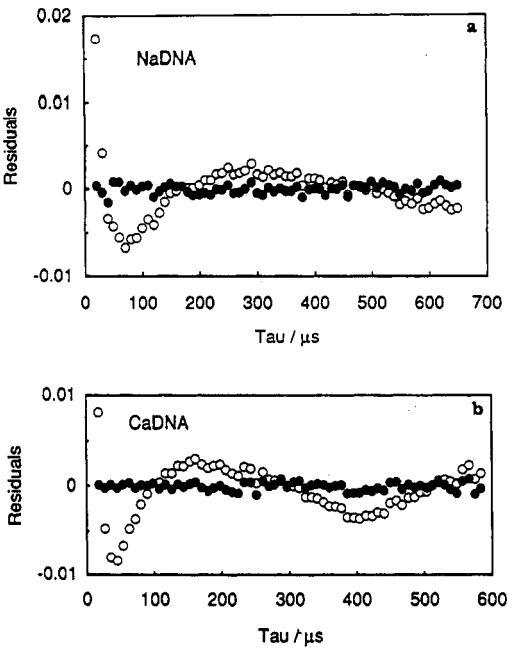

Figure 8. Residuals from cumulant analysis (open symbols) and biexponential fit (closed symbols) on long channel time data. (a) [NaDNA] = 8.2 mg/mL; (b) [CaDNA] = 7.9 mg/mL.

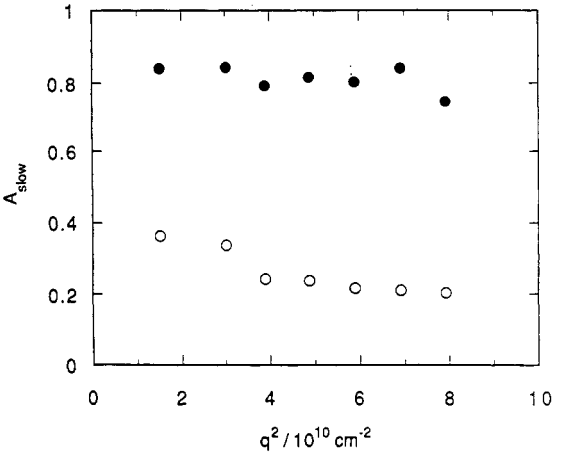

Figure 9. Amplitude of the slow component as a function of q^2 for (●) [NaDNA] = 8.2 mg/mL and (○) [CaDNA] = 7.9 mg/mL.

higher value of $D_{app,Ca}$ at long channel time discussed above, since D_{app} calculated from cumulant analysis is an average weighted by the amplitudes of the modes present.

At short channel times, correlation functions for NaDNA are better represented by a biexponential decay, while a single exponential obtained by cumulant analysis suffices for CaDNA. Two relaxation times probably are present but are too closely separated to be reliably fit using biexponential analysis. Halving Δt did not significantly change $D_{app,Ca}$.

The salt and DNA concentration dependences of D_{fast} and D_{slow} are summarized in Figures 10 and 11. Figure 10 shows that D_{fast} increases to a plateau value with decreasing salt and $D_{fast,Na} > D_{fast,Ca}$ at low salt. No salt concentration or counterion valence dependence is observed for D_{slow}. The same general trends are observed in the DNA concentration dependence (Figure 11) of D_{fast} and D_{slow}, with the main difference being the slight dependence of $D_{slow,Na}$ on DNA concentration.

These results are comparable, though different in some respects, with others on mononucleosomal DNA. Nicolai and Mandel[5] were unable to isolate a reproducible diffusion coefficient for D_{slow} but observed the presence of a slow mode for [NaCl] ≤ 0.01. Wang et al.[7] found a slow mode

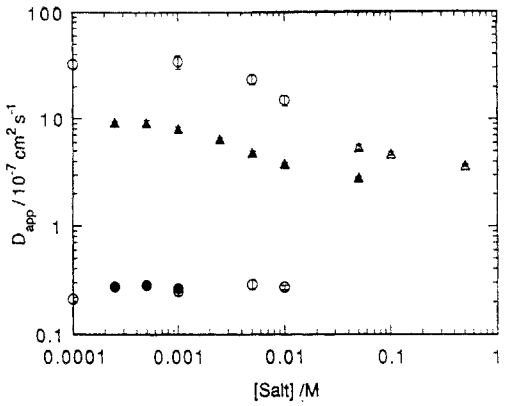

Figure 10. Salt concentration dependence of D_{fast} and D_{slow} obtained from biexponential (circles) and cumulant (triangles) analysis. [DNA] ≈ 8.5 mg/mL.

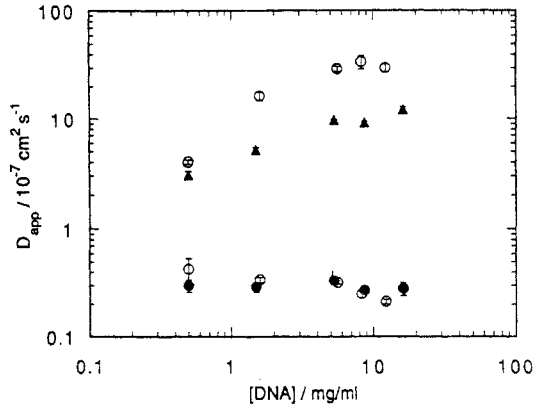

Figure 11. DNA concentration dependence of D_{fast} and D_{slow} obtained from biexponential (circles) and cumulant (triangles) analysis.

at salt concentrations as high as 1 M NaCl for DNA concentrations greater than ≈0.4 mg/mL. We were unable to detect a slow mode under these conditions.

The lack of dependence of D_{slow} on DNA or salt concentration contrasts with observations on flexible polyions. For PSS ($M_w = 1 \times 10^5$) at $C > 10C^*$, D_{slow} is independent of added salt. However, a decrease in D_{slow} with decreasing salt is noted for higher molecular weight PSS, ($M_w = 7.5 \times 10^5$)[18,19] and polylysine of $M_w = 2 \times 10^5$.[1,2] This may reflect swelling of the flexible polyion coil at very low salt. A large dependence on the polymer concentration is observed for PSS with $M_w > 10^5$.[18] D_{slow} decreases by 2 orders when the polyion concentration is varied in the range below C^* to greater than $10C^*$. However, no large dependence of D_{slow} on the polyion concentration is observed for salt-free PSS of $M_w = 1 \times 10^5$ when $C > C^*$.[18,20,21]

Use of the term "transition" to describe the emergence of the slow diffusion mode has led to the question: what are the critical conditions for the transition? Drifford and Dalbiez[18,19] obtained the expression

$$(C'_{mp}/2I)(1/\xi) = N \qquad (25)$$

relating the monomolar concentration C'_{mp} of polyion, ionic strength I, and counterion valence N at the onset of the slow mode. Equation 25 embodies the idea that the slow mode appears when the counterions contributed by the polyion exceed those contributed by the added salt. Note that the size of the polyion does not appear in this equation. It gives a good fit to data on polylysine and PSS.

We have applied eq 25 to DNA, as shown in Figure 12. For DNA, $C'_{mp} = [DNA]/M_u$, where [DNA] has units of g/L and M_u = 330 g/mol of bases (the molar mass of the

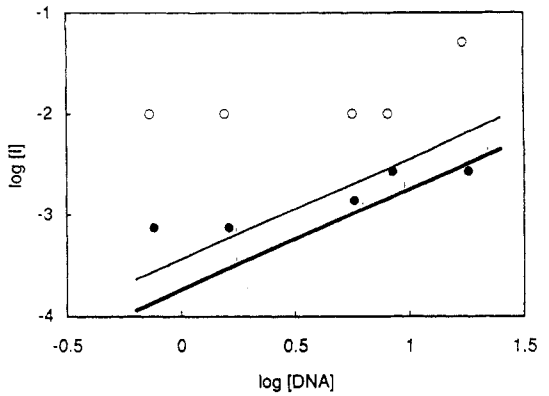

Figure 12. Comparison of the predicted (solid lines) and observed DNA and salt concentrations required for the appearance of the slow mode. The lines represent predictions from the Drifford relationship.

monomer carrying one structural charge). Though several studies with NaDNA have been done, this is the first with CaDNA, enabling a test of the counterion valence dependence of eq 25. Generally speaking, agreement between theory and experiment is poor, certainly not as good as obtained with flexible polyions. The slow mode appears at a lower [$CaCl_2$] relative to [NaCl], in agreement with the theory. However, the predicted linear relation between I and [DNA] does not hold, and the slow mode appears at lower [DNA] (or higher salt concentrations) than predicted.

The appearance of the slow decay for NaDNA is also more cooperative than that for CaDNA, showing less dependence on the salt or DNA concentration. To a certain extent, this is the result of our analysis procedure. The plotted concentrations are those at which we were able to obtain reproducible fits to extract the slow mode parameters. For NaDNA, this had not yet occurred at 50 mM NaCl (except at the highest [DNA]) and had occurred by 10 mM NaCl; we made no measurements at intermediate ionic strengths. Therefore, all but one of the NaDNA points are at I = 0.01 M. However, these results are also consistent with our general observations that the interactions in NaDNA are greater than those in CaDNA, as would be expected from the less well-shielded electrostatic interactions.

Another theory worth examining is that of van Veluwen et al.,[46] who proposed that two diffusion modes may arise in solutions of interacting colloidal particles if the solution has small amounts of polydispersity. The fast mode represents collective diffusion, and the slow mode represents exchange diffusion (i.e., diffusion of the local degree of polydispersity). The amplitude of the fast mode (A_+), relative to the total scattering amplitude $A_{tot} = A_+ + A_-$, is

$$A_+/A_{tot} = [(1 + (3\sigma^2\phi(4 - \phi))/(1 - \phi)^2)(1 + (3\sigma^2(7\phi^2 + 8\phi + 3))/(1 + 2\phi)^2)]^{-1} \qquad (26)$$

ϕ is the effective volume fraction of polymer, and σ is the polydispersity. As ϕ and σ increase, the fractional amplitude of the fast component decreases.

We relate the predictions made by eq 26 to the conditions required for observation of the slow mode in our experiments in the following way. We set σ = 0.031, the approximate breadth of the size distribution of our mononucleosomal preparation (160 ± 5 bp). The molar polymer concentration can be expressed in terms of ϕ:

$$C_p = M\phi/V_{eff}N_A \qquad (27)$$

V_{eff} is the effective polymer molecular volume in dm^3,

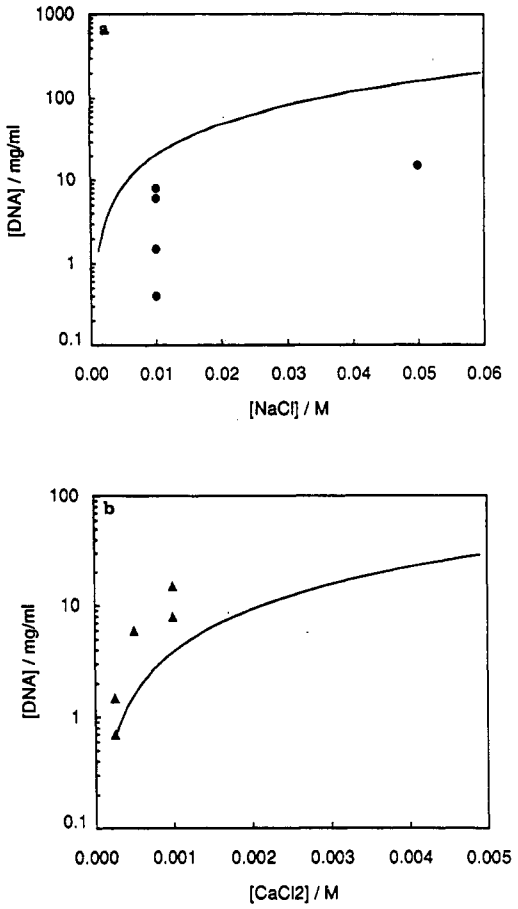

Figure 13. Predicted and observed DNA concentrations corresponding to (a) $\Phi_{Na} = 0.97$ and (b) $\Phi_{Ca} = 0.85$. The solid curve is based on exchange diffusion theory of van Veluwen et al. (1987).

$\pi R_{eff}^2 L_{eff}$, where R_{eff} and L_{eff} are the effective radius and length of the polyion. R_{eff} and L_{eff} are dependent on the salt concentration and are calculated using eqs 10 and 12. A_+/A_{tot} is calculated from eq 26 for values of ϕ in the range 0.50–0.98. We then choose the value of ϕ corresponding to the experimentally observed A_-, where $A_- = A_{tot} - A_+$. For CaDNA, $A_{slow} \approx 0.3$ in the region of the salt concentration where the slow mode appears, and for NaDNA, $A_{slow} \approx 0.8$. These correspond to $\phi_{Na} \approx 0.97$ and $\phi_{Ca} \approx 0.85$. V_{eff} is then determined for the range of salt concentrations investigated. Figure 13 compares the values of C_p calculated using eq 27 with the DNA concentrations necessary to observe the slow mode in CaDNA and NaDNA. The predicted DNA concentrations giving $\phi_{Ca} = 0.85$ are not far from those where the slow mode is observed. However, for NaDNA the slow mode appears at considerably lower values of [DNA] than predicted, indicating some inadequacy in the theory.

Another possibility is that the slow mode arises not from inherent small sample polydispersity but instead from a mixture of a large aggregate and single DNA rods. The aggregate could arise from an ordered structure of polyions stabilized in some manner by low salt (the temporal aggregate model[43]). Alternatively, it might be an impurity present in very low amounts, whose contribution to the scattering becomes perceptible only when the scattering from the DNA is sufficiently reduced by virial coefficient effects at very low salt[59] (Peitzsch et al., 1992). In either case, the hydrodynamic radius of the putative aggregate calculated from D_{slow} is 750 Å. (This seems to render the impurity hypothesis unlikely, since all solutions were passed through 0.22-nm filters before scattering.) If the aggregate is an ordered DNA array, the number of molecules/aggregate, n_{agg}, can be estimated from the interparticle spacing, d_{int}, obtained by small-angle X-ray scattering.[35] From the scattering vector of the intensity maximum at low salt, we find $d_{int} \approx 76$ Å. Assuming parallel orientation of the DNA molecules, $n_{agg} \approx (2R_{agg}/d_{int})^2 \approx 400$. To estimate the scattering behavior of such a monomer–aggregate mixture would require knowing the scattering amplitude of the aggregate as a function of ionic strength. Unfortunately, such knowledge (either experimental or theoretical) is lacking. However, even allowing for substantial diminution in the scattering power per monomer in the aggregate, relative to free monomer, the M^2 dependence of the scattering intensity would mean that a small fraction of material in aggregated form could dominate the scattering in the way observed.

Summary

Our comparisons of NaDNA with CaDNA showed that, in all types of experiments, there was a dependence on counterion valence that did not simply reflect ionic strength. In the ordinary regime, there was generally qualitative agreement with standard theories, but quantitative agreement was not good. Effective linear charge densities needed to reproduce experimental results deviated in opposite directions from theoretical predictions for static and dynamic light scattering experiments.

In the extraordinary regime, electrostatic interactions for CaDNA are weaker than for NaDNA, as expected; but the ordinary–extraordinary transition is also less abrupt with Ca, which was not necessarily expected. We find that the interactions driving the transition are stronger than those predicted from the relationship proposed by Drifford and Dalbiez;[18,19] this may reflect the difference between flexible and rodlike polyelectrolytes. The polydispersity theory proposed by van Veluwen et al.[46] can account at least semiquantitatively for the existence of a slow mode, but only by allowing the effective polyion volume fraction to approach unity. While this is not inconsistent with the concept of a greatly expanded ion atmosphere around a polyion at low ionic strength, it may be pushing the concept beyond its range of validity. The presence of an aggregate is perhaps the most intuitively plausible explanation for the extraordinary phase, since an aggregate with the size needed to give D_{slow} and with the local concentration given by SAXS measurements would have relatively great scattering power even if such aggregates were rare. The major problem with this explanation is that the forces stabilizing the aggregate are obscure.

References and Notes

(1) Lee, W. I.; Schurr, J. M. *J. Polym. Sci., Polym. Phys. Ed.* **1975**, *13*, 873.
(2) Lin, S.-C.; Lee, W. I.; Schurr, J. M. *Biopolymers* **1978**, *17*, 1041.
(3) Fulmer, A. W.; Benbasat, J. A.; Bloomfield, V. A. *Biopolymers* **1981**, *20*, 1147.
(4) Schmitz, K. S.; Lu, M. *Biopolymers* **1984**, *23*, 797.
(5) Nicolai, T.; Mandel, M. *Macromolecules* **1989**, *22*, 2348.
(6) Nicolai, T.; Mandel, M. *Macromolecules* **1989**, *22*, 438.
(7) Wang, L.; Garner, M. M.; Yu, H. *Macromolecules* **1991**, *24*, 2368.
(8) Goinga, H. T.; Pecora, R. *Macromolecules* **1991**, *24*, 6128.
(9) Tivant, P.; Turq, P.; Drifford, M.; Magdelenat, H.; Menez, R. *Biopolymers* **1983**, *22*, 643.
(10) Ackerson, B. J. *J. Chem. Phys.* **1978**, *69*, 684.
(11) Stephen, M. J. *J. Chem. Phys.* **1971**, *55*, 3878.
(12) Berne, B. J.; Pecora, R. *Dynamic Light Scattering with Applications to Chemistry, Biology, and Physics*; Wiley-Interscience: New York, 1976; p 376.
(13) Patkowski, A.; Gulari, E.; Chu, B. *J. Chem. Phys.* **1980**, *73*, 4178.
(14) Schmitz, K. S.; Lu, M. *Proc. Natl. Acad. Sci. U.S.A.* **1983**, *80*, 425.

(15) Koene, R. S.; Mandel, M. *J. Mol. Biol.* **1983**, *196*, 220.
(16) Koene, R.; Mandel, M. *Macromolecules* **1983**, *16*, 973.
(17) Drifford, M.; Dalbiez, J.-P. *J. Phys. Chem.* **1984**, *88*, 5368.
(18) Drifford, M.; Dalbiez, J.-P. *Biopolymers* **1985**, *24*, 1501.
(19) Drifford, M.; Dalbiez, J. P. *J. Phys. Lett.* **1985**, *46*, L-311.
(20) Mathiez, P.; Weisbuch, G.; Mouttet, C. *Biopolymers* **1979**, *18*, 1465.
(21) Schmidt, M. *Makromol. Chem., Rapid Commun.* **1989**, *10*, 89.
(22) Schmitz, K. S. *Biopolymers* **1982**, *21*, 1383.
(23) Schurr, J. M.; Schmitz, K. S. *Annu. Rev. Phys. Chem.* **1986**, *37*, 271.
(24) DeLong, L. M.; Russo, P. S. *Macromolecules* **1991**, *24*, 6139.
(25) Shibata, J.; Schurr, J. M. *Biopolymers* **1979**, *18*, 1831.
(26) Martin, N. B.; Tripp, J. B.; Shibata, J. H.; Schurr, J. M. *Biopolymers* **1979**, *18*, 2127.
(27) Wilcoxon, J. P.; Schurr, J. M. *J. Chem. Phys.* **1983**, *78*, 3354.
(28) Zero, K.; Ware, B. R. *J. Chem. Phys.* **1984**, *80*, 1610.
(29) Schmitz, K. S.; Ramsay, D. J. *Biopolymers* **1985**, *24*, 1247.
(30) Reed, W. F.; Ghosh, S.; Medjahdi, G.; Francois, J. *Macromolecules* **1991**, *24*, 6189.
(31) Ramsay, D. J.; Schmitz, K. S. *EMBO J.* **1985**, *2*, 2422.
(32) Mandelkern, M.; Dattagupta, N.; Crothers, D. M. *Proc. Natl. Acad. Sci. U.S.A.* **1981**, *78*, 4294.
(33) Stigter, D. *Biopolymers* **1979**, *18*, 3125.
(34) Onsager, L. *Ann. N.Y. Acad. Sci.* **1949**, *51*, 627.
(35) Wang, L.; Bloomfield, V. A. *Macromolecules* **1991**, *24*, 5791.
(36) Strzelecka, T. E.; Rill, R. L. *Biopolymers* **1990**, *30*, 57.
(37) Strzelecka, T. E.; Rill, R. L. *Macromolecules* **1991**, *24*, 5124.
(38) Doi, M.; Shimada, T.; Okano, K. *J. Chem. Phys.* **1988**, *88*, 4070.
(39) Schulz, S. F.; Maier, E. E.; Weber, R. *J. Chem. Phys.* **1989**, *90*, 7.
(40) Ise, N.; Okubo, T.; Yamamoto, K.; Matsuoka, H.; Kawai, H.; Hashimoto, T.; Fujimura, M. *J. Chem. Phys.* **1983**, *78*, 541.
(41) Ise, N.; Okubo, T.; Yamamoto, K.; Matsuoka, H.; Kawai, H.; Hashimoto, T.; Fujimura, M.; Hiragi, Y. *J. Am. Chem. Soc.* **1980**, *102*, 7901.
(42) Levij, M.; DeBleijser, J.; Leyte, J. C. *Chem. Phys. Lett.* **1981**, *83*, 183.
(43) Schmitz, K. S.; Lu, M.; Singh, N.; Ramsay, D. J. *Biopolymers* **1984**, *23*, 1637.
(44) Overbeek, J. T. C. *J. Chem. Phys.* **1987**, *87*, 4406.
(45) Pusey, P. N.; Fijnaut, H. M.; Vrij, A. *J. Chem. Phys.* **1982**, *77*, 4270.
(46) van Veluwen, A.; Lekkerkerker, H. N. W.; de Kruif, C. G.; Vrij, A. *Faraday Discuss. Chem. Soc.* **1987**, *83*, 59.
(47) Benmouna, M.; Benoit, H.; Duval, M.; Akcasu, Z. *Macromolecules* **1987**, *20*, 1107.
(48) Wang, L.; Ferrari, M.; Bloomfield, V. A. *BioTechniques* **1990**, *9*, 24.
(49) Gallagher, W. H.; Woodward, C. K. *Biopolymers* **1989**, *28*, 2001.
(50) Bloomfield, V. A.; Lim, T. K. *Methods Enzymol.* **1978**, *48F*, 415.
(51) Koppel, D. E. *J. Chem. Phys.* **1972**, *57*, 4814.
(52) Press, W. H.; Flannery, B. P.; Teukolsky, S. A.; Vetterling, W. T. *Numerical Recipes: The Art of Scientific Computing*; Cambridge University Press: Cambridge, U.K., 1986.
(53) Tanford, C. *Physical Chemistry of Macromolecules*; John Wiley & Sons, Inc.: New York, 1961.
(54) Utiyama, H. In *Light Scattering from Polymer Solutions*; Huglin, M. B., Ed.; Academic Press: New York, 1972; p 61.
(55) Manning, G. S. *Q. Rev. Biophys.* **1978**, *11*, 179.
(56) Tirado, M. M.; Garcia de la Torre, J. *J. Chem. Phys.* **1979**, *71*, 2581.
(57) Rhee, K. W.; Ware, B. R. *J. Chem. Phys.* **1983**, *78*, 3349.
(58) Peterson, J. M.; Fixman, M. *J. Chem. Phys.* **1963**, *39*, 2516.
(59) Li, X.; Reed, W. *J. Chem. Phys.* **1991**, *94* (6), 4568.